This is a preprint, the final version is subject to change, of the American Mineralogist (MSA)
Cite as Authors (Year) Title. American Mineralogist, in press.
DOI: https://doi.org/10.2138/am-2020-6995

REVISION 1

Celestine discovered in Hawaiian basalts

Garcia, Michael O., and Hellebrand, Eric*

Department of Earth Sciences, University of Hawai'i at Mānoa, Honolulu, HI 96822, USA

ABSTRACT

We report here the first occurrence of celestine in recent oceanic basalts. Celestine was found in moderately altered accidental volcanic blocks from Ka'ula Island, a rejuvenated tuff cone in the northern Hawaiian Islands. This occurrence is novel not only for the presence of celestine but also for the absence of barite, the sulfate mineral most commonly found in oceanic hydrothermal deposits. Celestine was found lining vesicles and partially fillings voids within the matrix of several high Sr (2200-6400 ppm) Ka'ula basalts. High-quality wavelength dispersive microprobe analyses of celestine are reported here for near end-member celestine (>90%). The Ka'ula celestine deposits are compositionally heterogeneous with large variations in Ba content (0.9-7.5 wt.%) within single mineral aggregates. The mostly likely source of the Sr for celestine in the Ka'ula basalts was the host basalt, which contains ~1200 ppm. This is about 10 times higher than normally found in mid-ocean ridge basalts and 4 times greater than commonly observed in Hawaiian basalts. Hydrothermal alteration by S-bearing fluids related to the eruption that transported these accidentally fragments probably mobilized Sr in the blocks. These S-rich solutions later precipitated celestine during or following the eruption. We were unable to confirm the origin for the Sr via Sr isotope measures because the Ka'ula celestine was too fine grained, friable and widely dispersed to be concentrated for Sr isotope analyses. Future studies of basalts from active volcanoes on oceanic islands, especially for basalts with elevated Sr contents (>1000 ppm), should be aware of the possible presence of celestine in moderately altered lavas.

Keywords: Hawaii, volcanic rocks, celestine, hydrothermal alteration, strontium

*current address: Department of Earth Sciences, Utrecht University, Budapestlaan 4, 3584CD Utrecht, The Netherlands

This is a preprint, the final version is subject to change, of the American Mineralogist (MSA)
Cite as Authors (Year) Title. American Mineralogist, in press.
DOI: https://doi.org/10.2138/am-2020-6995

INTRODUCTION

Celestine ($SrSO_4$) is normally associated with continental evaporate deposits, although it is also reported in hydrothermally altered continental volcanic and intrusive rocks (even kimberlites and lamproites) as well as in some metamorphic rocks (eclogites; Hanor, 2000; Karakaya et al. 2001; Bailey and Lupulescu, 2007; Nakamura et al., 2010; Rukhlov et al., 2013; Anenburg et al. 2014; Nickschick et al., 2014; Enkhbayar et al., 2016). In sedimentary environments, celestine is thought to form by reaction of hypersaline Sr-rich fluids with gypsum and/or anhydrite (Hanor, 2000). In continental igneous settings, celestine is commonly associated with barite and the two are interpreted to be the product of interaction of a hydrous silicate fluid (rich in Sr and Ba) with a sulfur-rich fluid (Hanor, 2000). Celestine is an important ore mineral (the principle commercial source for Sr). The principal uses of celestine in the USA are: drilling fluids (70%); ceramic ferrite magnets, and pyrotechnics and signals (9% each), electrolytic production of zinc, master alloys, pigments and fillers, and other applications, including glass (3% each; U.S. Geological Survey, 2019). Celestine is apparently unreported from active oceanic volcanic regions (e.g., mid-ocean ridge hydrothermal vents) and was unknown in the Hawaiian rocks prior to its accidental discovery in high Sr content (2200-6400 ppm) lavas from Kaʻula Island (Fig. 1; Garcia et al., 2016). However, high Sr content barite (11-12 wt.% SrO) was reported in hydrothermal deposits related to the 1996 eruption of Lōʻihi volcano, a seamount located south of the island of Hawaiʻi (Davis and Clague, 1998; Davis et al., 2003), and in mid-ocean ridge hydrothermal vent deposits (e.g., Loki's Castle; Eickmann et al., 2014). Celestine was not reported at either of these areas. The Kaʻula occurrence presents a rare opportunity where an explosive eruption tapped moderately hydrothermally altered submarine basalts (Garcia et al., 1986). Although no barite was found in these Kaʻula rocks, earlier formed, Ba-bearing zeolite (phillipsite with up to 2 wt% BaO) is present (Garcia et al., 2016).

Here we document the mode of occurrence of celestine in Kaʻula Island basalts using backscattered electron imagery, present high precision electron microprobe analyses of celestine, examine the effects of alteration on the geochemistry of Kaʻula basalts, and discuss possible origins for the formation of celestine in these rocks. High precision analyses of near endmember celestine are rare in the scientific literature; most reported compositions are based on lower precision, EDS analyses (e.g., Anenburg et al., 2014; Garcia et al., 2016) or wavelength dispersive (WDS) analyses with undocumented analytical conditions or poor totals (<99 wt.% or >100.8 wt.%; e.g., Fernández-Cortés et al., 2006; Xu et al., 2010; Burtseva et al., 2013). Celestine is normally undersaturated with respect to hydrothermal solutions in marine

environments, suggesting that the presence of celestine is not the result of thermodynamically controlled precipitation (Hanor, 2000; Singer et al., 2016). However, the very high Sr content of these unaltered Ka‘ula basalts (~1200 ppm) compared to other oceanic basalts (e.g., 100-150 ppm in mid-ocean ridge basalts; Hemond et al., 2006) may be the key factor in favoring precipitation of celestine over barite in the Ka‘ula basalts. Hydrothermal S-rich solutions related to the eruption that carried the basalt blocks to the surface was probably responsible for the formation of celestine at Ka‘ula.

GEOLOGICAL SETTING

Ka‘ula Island is a small (~1 km long), crescent-shaped remnant of a tuff cone that forms the crown of a small, independent Hawaiian shield volcano (Fig. 1), the oldest of the main Hawaiian volcanoes (~6.25 Ma; Garcia et al., 1986; 2016). The island is located near the summit of Ka‘ula shield volcano and along its southeast rift zone (Fig. 1). The cone is part of an extensive field of rejuvenation stage volcanoes that formed more than 2 Myrs after the underlying shield volcano stopped erupting (Garcia et al., 2016). An extensive field of rejuvenation stage cones and associated lava flows forms a broad apron ~50 km wide surrounding the shield (Garcia et al., 2008; 2016). An accidental basalt block from the island and seven submarine basalts collected during two JASON ROV dives on the broad apron yielded ^{40}Ar-^{39}Ar ages of 0.55-1.95 Ma for Ka‘ula rejuvenation stage volcanism (Garcia et al., 2016). The age of the eruption that formed Ka‘ula island is unknown but <0.66 Ma based on dating of an accidental block from the tuff cone. The high Sr content basalt samples (2270 to 6400 ppm) examined in this study (KA-17, KA-19 and KA-34) were accidental blocks in the tuff cone derived from earlier rejuvenation stage eruptions. The composition of these blocks is strongly alkaline basalts (basanite and foidite; Garcia et al., 1987; 2016), which are typical of Hawaiian rejuvenate stage lava (e.g., Clague and Frey, 1982). The Sr content of fresh basanite and foidites from other Hawaiian Islands (Kaua‘i and O‘ahu) ranges from 500 to 1600 ppm, although a strongly alkaline lava from O‘ahu, a melilite-bearing foidite with ~36 wt.% SiO_2, has up to 3000 ppm Sr (e.g., Clague and Frey, 1982; Fekiacova et al., 2007; Garcia et al., 2010). Finding a lava with more than twice the Sr content ever reported in a Hawaiian basalt (KA-19 with 6400 ppm Sr) was surprising (Garcia et al., 2016). The cause of anomalously high Sr in these Ka‘ula rocks was the subject of this study.

METHODS

Backscattered electron (BSE) images and compositional analyses were acquired using the University of Hawai‘i JEOL 8500 Hyperprobe electron microprobe equipped with five,

wavelength dispersive spectrometers. Operating conditions were a beam energy of 15 keV with a 5 nA beam current and 3 micrometer diameter. The low beam current was necessary because of the small beam diameter that was needed to document the composition of the fine grained (<5-20 μm) celestine crystals. Elements were acquired using analyzing crystals LiFH (H for large crystal) for Ba L-alpha and Fe K-alpha, PETH for S K-alpha, PET for Sr L-alpha and Ca K-alpha, and TAP for Si K-alpha lines. The counting time were 20 seconds for Ba and Fe, 30 seconds for Si, and 50 seconds for Ca, S, and Sr. The standards were UCLA Diopside for Ca and Si, benitoite for Ba, Staunton meteorite troilite for Fe, strontianite for Sr, and a nearly pure celestine for S ka (Table 1). Detection limits the minor elements in celestine were 0.02 wt.% for Si, 0.1 wt.% for Fe, and 0.16 wt.% for Ba based on counting statistics. Analytical precision (at the 99% confidence level) ranged from 0.60 percent relative for S to 2.5 percent relative for Ca based on repeated measurements of standards. Oxygen was calculated by cation stoichiometry and included in the matrix correction. A ZAF matrix correction method (Armstrong, 1988) was applied to process the raw data to yield concentration values. Structural formula were calculated for our celestine analyses to demonstrate the near end-member composition of the Kaula celestine (>90% celestine component for 13 of 15 analyses) and the high data quality (cation totals of 2.000 ±0.035, mostly within ±0.020; Table 1).

Whole-rock XRF major and trace element (Ba, Rb, Sr, Y, Zr, Nb, Ba, Zn, Ni, Cr, and V) analyses of four of the five basalts used in this study were originally reported in Garcia et al. (1987). They were reanalyzed for this study along with a new sample, KA-16, in the same lab at the University of Massachusetts as previously used but with enhanced detection instrumentation. In addition, the Ka‘ula submarine basalts used for comparison with the Kaula Island basalts in this study were analyzed in the same lab a few years earlier. For the XRF procedural methods and analytical precision, see Rhodes and Vollinger (2004). All of the basalt samples were coarsely crushed (1-8 mm) with a tungsten-carbide coated hydraulic press, ultrasonically cleaned in Millipore water, then dried for 24 hours at 40 °C followed by powdering in a tungsten-carbide mill.

RESULTS

Petrography

The Ka‘ula celestine-bearing basalts are basanites (41-43 wt.% SiO_2 with 3-5 wt.% total alkalis; Garcia et al., 2016). They contain abundant olivine 10-15 vol.% in a mostly cryptocrystalline matrix with clinopyroxene, magnetite and rare mantle-derived olivine and clinopyroxene megacrysts. Many of the vesicles and other voids in the matrix are partially filled

with phillipsite (Fig. 2a). Celestine was discovered using backscattered electron imagery (Fig. 2). The distribution of celestine is patchy. It occurs partially filling vesicles (along with earlier formed phillipsite) and in matrix voids of the Ka‘ula accidental volcanic blocks (Fig. 2c). Celestine was also found to be incipiently replacing the rim of unaltered olivine crystals (Fig. 2d). X-ray maps were made of several areas with well-developed celestine (Figs. 3). The maps of Sr and Ba show the complex distribution of both elements in the Ka‘ula celestine aggregates (Fig. 2). The brighter areas in the BSE image have higher Ba and lower Sr contents than the darker areas (Fig. 2).

Chemistry

Celestine forms a solid solution with barite, with each mineral typically containing only minor components of the other endmember (e.g., celestine usually contains less than 4 mole% $BaSO_4$; Hanor, 1968, 2000). There are, however, reports of celestine with up to 20 wt.% BaO in lamproite deposits (Rukhlov et al., 2013). Celestine normally contains impurities of Ca (up to 2000 ppm) and FeO (up to >1 wt.%), and traces of Si, REE and Pb (Hanor, 2000; Anenburg et al., 2014), although most previous analyses of celestine don't report all of these elements.

The Ka‘ula celestines range from 84-100% endmember celestine ($SrSO_4$; Cs), although 14 of 15 analyses have >90% Cs (Table 1). These values span nearly the entire range reported in the Hanor (2000) synthesis on celestine and barite (74-100% Cs), although only two of these earlier analyses have <84% Cs. BaO content in the Ka‘ula celestines is highly variable (0.1-7.5 wt.%) even within localized areas (e.g., single vesicle; Fig. 3; Table 1). Compositional diversity was initially detected in BSE images with darker and lighter patches within celestine aggregates. The darker patches contain less Ba than the lighter patches (0.9- 2.4 vs. up to 7.5 wt.% BaO; Table 1, Fig. 3). Iron contents are low (<0.1-0.6 wt.% FeO), as is SiO_2 (<0.1-0.9 wt.% but mostly <0.3 wt.%). CaO is somewhat more abundant (0.6-2.5 wt.%). None of these oxides show any correlation with Ba content in the Ka‘ula celestine (Table 1). These new analyses (Table 1) are the some of the first high precision analyses of celestine reported in the peer-reviewed literature based on the sum of the oxide totals (13 of 15 analyses are 99.0-100.5 wt.% and cation totals of 2.000 ± 0.020; Table 1). Many previously reported celestine analyses were based on EDS methods (Anenburg et al., 2014; Garcia et al., 2016), although some WDS analyses are available for non-basalt hosted samples (e.g., Xu et al., 2010 and Burtseva et al., 2013 for a carbonatite occurrences; Nakamura et al., 2010, for a eclogite sample). However, the analytical

methods described in these papers are incomplete, some of the oxide totals are not good and no structural formula are given.

The new XRF analyses using more precise methods than we previously reported (Garcia et al., 1986) yielded somewhat different major and trace element compositions. In general, the new analyses (Table 2) have somewhat higher Ba and Zr contents and lower Rb. The differences in these analyses are also affected by the heterogeneous nature of these basalts, which contain a patchy distribution of secondary minerals. LOI values for these new analyses range from 0.2-4.7 wt.% (Table 2), indicating mild to moderate levels of alteration. This is consistent with the petrographic observations that show common secondary mineral formation but also fresh olivine in areas not affected by secondary mineralization (Fig. 2).

DISCUSSION

Hydrothermal Alteration of Ka‘ula Accidental Blocks

The concentration of Sr in some Ka‘ula rocks is 2-4 times greater than previously observed in any Hawaiian rejuvenated lavas of similar composition or predicted based on the abundance of other similarly incompatible elements (e.g., Zr and Ti) and even highly incompatible elements (e.g., Ba and Nb; Garcia et al., 2016). To evaluate the cause of the high Sr concentration in the Ka‘ula Island accidental blocks, we examined them petrographically and compared their incompatible elements concentrations with unaltered Ka‘ula submarine basanitic pillow basalts.

Petrographically, the basanitic blocks from Ka‘ula Island have undergone weak to moderate levels of alteration. The blocks appear relatively unaltered in hand specimen and thin section except for the partial filling of some vesicles with phillipsite. Another indication of their alteration level is their low to moderate loss-on-ignition (LOI) values of 0.4-2.8 wt.% (Table 2). Sample KA-19 has the most Sr (6400 ppm; previous value was 5384 ppm; Garcia et al., 1997) and highest LOI (2.8 wt.%). There is a positive correlation of LOI with Sr content in these island blocks (Table 2). Comparing them with unaltered submarine Ka‘ula pillow basalts (LOI values average 0.35 wt.%) with similar SiO_2 (41.7 wt.%) and MgO (12 wt%) contents reveals some significant geochemical differences between the altered island and fresh submarine basalts (Table 2; Fig. 4). Two trends are evident in this comparison. The sample with the highest Sr content (KA-19), shows depletion in incompatible elements (Rb, Ba, and Nb) with little or no change in Zr, Ti and Y (Fig. 4). Thus, the water soluble elements (K, Rb) are depleted in the most altered island basalt. The other samples show a mild enrichment in Ba, that is probably related to the

presence of Ba-bearing zeolites in these samples (Garcia et al., 2016). Sr enrichment progressively increased with Ba enrichment (except for the sample KA-19) and with Rb depletion. The increase in Sr in these more weakly altered rocks may be related to phillipsite formation, which contains up to 3.3 wt.% SrO (Garcia et al., 2016). Thus, the alteration of the Ka‘ula island blocks may have involved two stages of alteration. During the first stage, Ba- and Sr-bearing phillipsite formed occupying most vesicles in the Ka‘ula Island samples. The second stage involved the enrichment in Sr and depletion in Ba as celestine filled voids in the matrix and some vesicles, overprinting the earlier increase in Ba from phillipsite crystallization.

The absence of barite in the Ka‘ula basalts is anomalous compared to other submarine areas that contain sulfate minerals (e.g., Davis et al., 2003; Eickmann et al., 2003). Normally, barite is present with minor or no celestine (Hanor, 2000; Singer et al., 2016). Celestine is normally undersaturated in hydrothermal solutions, suggesting its presence at Ka‘ula may not be the result of only thermodynamically controlled precipitation (e.g., Singer et al., 2016). Typically, Ba is preferentially removed from a hydrothermal solution resulting in a Sr-poor solid phase (e.g., barite or anhydrite). Continued precipitation in a closed system may result in a solution enriched in Sr and subsequent precipitation of a more Sr-rich phase, especially if the solution temperature increased because of the retrograde solubility of celestine (Hanor, 2000). However, there are occurrences in altered continental igneous rocks of celestine with no barite (basalts and carbonatites; Anenburg et al., 2014; Nickschick et al., 2014), although the two sulfate minerals commonly occur together (e.g., Nickschick et al., 2014). Celestine formation in the basalt was related to hydrothermal activity from a dike intruding carbonaceous sediments, which were the source of the Sr. In a zoned carbonatite complex, celestine formation was related to metasomatism by a sulfate-rich fluid from late stage magmatic activity (Enkhbayar et al., 2016).

The source of the very high Sr concentrations in some Ka‘ula island basalts that contain celestine was most likely the host lava, similar to carbonatite example noted above (Enkhbayar et al., 2016). There is no other source for excess Sr is known at this location. For example, no carbonate material has been recovered from the tephra or known on the volcanic ediface. Ka‘ula island is located near the summit of Ka‘ula shield volcano (Fig. 1). Thus, it is a prime site for hydrothermal activity. The most likely scenario for celestine formation in the island basalts is hydrothermal S-rich acidic solutions related to the eruption that formed the island. These solutions probably leached Sr from the strongly silica undersaturated basalts with elevated Sr contents (~1200 ppm). Subsequently, celestine was precipitated in the voids of these Ka‘ula island basalts during or after the eruption that formed the island. Additionally or alternatively, the

early formation of Ba-rich phillipsite (Garcia et al., 2016) may have enriched the hydrothermal solutions in Sr.

The unusually high Sr abundance in strongly silica understaturated Ka‘ula rocks compared to mid-ocean ridge basalts (100-150 ppm; Hemond et al., 2006) vs. 1200 ppm (Garcia et al., 2016) may have led to the preferential formation of celestine over barite. Thus, the high Sr abundance in fresh rejuvenated Ka‘ula basalts may have led to this unusual and possibly unique occurrence of celestine in the modern ocean basins.

IMPLICATIONS

The presence of celestine and absence of barite in the Ka‘ula Island accidental basalt blocks represents a novel discovery in modern oceanic basalts. Barite is normally observed and is thermodynamically favored in most hydrothermal solutions (Hanor, 2000). Future studies of hydrothermally altered basalts from active volcanoes on oceanic islands, especially for basalts with elevated Sr contents (>1000 ppm), should be aware of the possible presence of celestine in moderately altered lavas.

ACKNOWLEDGEMENTS

We thank Michael Vollinger for expert XRF analyses of the Ka‘ula rocks, David Grooms for collecting these basalts from Ka‘ula Island (an active U.S. military bombing target), and the anonymous reviewers of this manuscript. Funding for this study was provided by U.S. National Science Foundation grant, OCE-1737284 to M.G. This paper is SOEST contribution number xxxxx.

REFERENCES CITED

Anenburg, M., Bialik, O.M. Vapnik, Y, Chapman, H.J., Antler, Katzir, G.Y. and Bickle, M.J., (2014) The origin of celestine–quartz–calcite geodes associated with a basaltic dyke, Makhtesh Ramon, Israel. Geological Magazine, 151, 798–815.

Armstrong J.T. (1988) Quantitative analysis of silicate and oxide materials: Comparison of Monte Carlo, ZAF, and rho(pz) procedures. In Microbeam Analysis (ed. D.E. Newbury). San Francisco Press, San Francisco, 239-246.

Bailey, D.G. and Lupulescu, M.V. (2007) Kimberlitic Rocks of Central New York. Field Trip Guidebook for the 79th Annual Meeting of the New York State Geological Association, 53-81.

Burtseva, M.V., Ripp, G.S. and Doroshevich, A.G. (2013). Features of mineral and chemical composition of the Khamambettu carbonatites, Tamil Nadu. Journal Geological Society of India, 81, 655-664.

Clague D.A., Frey F.A., Garcia M.O., Huang S., McWilliams M., and Beeson M.H. (2016) Compositional Heterogeneity of the Sugarloaf Melilite Nephelinite Flow, Honolulu Volcanics, Hawaii. Geochimica Cosmochimca et Acta, http://dx.doi.org/10.1016/j.gca.2016.01.034.

Clague D.A. and Frey F.A. (1982) Petrology and trace element geochemistry of the Honolulu Volcanics, Oahu: Implications for the oceanic mantle below Hawaii. Journal of Petrology, 23, 447-504.

Davis, A.S. and Clague, D.A. (1998) Changes in the hydrothermal system at Loihi Seamount after the formation of Pele's pit in 1996. Geology, 26, 399–402.

Davis, A.S., Clague, D.A., and Zierenberg, R.A., Wheat, C.G., Cousens, B.L. (2003) Sulfide formation related to changes in the hydrothermal system on Loihi Seamount, Hawaii, following the seismic event in 1996. Canadian Mineralogist, 41, 457–472.

Eickmann, B. Thorseth, H., Peters, M., Strass, H., Brocker, M., and Pedersen, R.B. (2014) Barite in hydrothermal environments as a recorder of subseafloor processes: a multiple-isotope study from the Loki's Castle vent field. Geobiology, 12, 308–321.

Enkhbayar, D., Seo, J., Choi, S.-G., Lee, Y.J. and Batmunkh, E. (2016) Mineral Chemistry of REE-Rich Apatite and Sulfur-Rich Monazite from the Mushgai Khudag, Alkaline Volcanic-Plutonic Complex, South Mongolia. International Journal of Geosciences, 7, 20-31, doi.org/10.4236/ijg.2016.71003

Fekiacova Z., Abouchami W., Galar S.J.G., Garcia M.O., and Hofmann A.W. (2007) Origin and temporal evolution of Ko'olau Volcano, Hawai`i: Inferences from isotope data on the Ko'olau Scientific Drilling Project (KSDP), the Honolulu Volcanics and ODP Site 843. Earth and Planetary Science Letters, 261, 65-83.

Fernández-Cortés, Á., Calaforra, J.M., García-Guinea, (2006) The Pulpí gigantic geode (Almería, Spain): geology, metal pollution, microclimatology, and conservation. Journal of Environmental Geology, 50, 707

Garcia M.O., Frey F.A. and Grooms D. (1986) Petrogenesis of volcanic rocks from Kaula Island, Hawaii: Implications for the origin of Hawaiian phonolites. Contribution to Mineralogy and Petrolrology, 94, 461-471.

Garcia, M.O. et al. (2008) Widespread secondary volcanism near the northern Hawaiian Islands. Eos Transactions American Geophysical Union, 89, 542-543.

Garcia M.O., Swinnard L., Weis D., Greene A.R., Tagami T., Sano H. and Gandy C.E. (2010) Petrology, Geochemistry and Geochronology of Kaua'i Lavas over 4.5 Myr: Implications for the Origin of Rejuvenated Volcanism and the Evolution of the Hawaiian Plume. Journal of Petrology, 51, 1507–1540.

Garcia, M.O., Weis, D., Jicha, B.R., Ito, G., and Hanano, D. (2016) Petrology and geochronology of lavas from Ka'ula Volcano: Implications for rejuvenated volcanism of the Hawaiian Mantle Plume. Geochimica et Cosmochimica Acta, 185, 278–301, doi.org/10.1016/j.gca.2016.03.025.

Hanor, J.S. (2000) Barite–Celestine geochemistry and environments of formation. Reviews of Mineralogy and Geochemistry, 40, 193–275.

Hanor, J. (1968) Frequency distribution of compositions in barite-celestite series. American Mineralogist, 53, 1215-1222.

He´mond, C., Hofmann, A.W., Vlaste´lic, I. and Nauret, F. (2006) Origin of MORB enrichment and relative trace element compatibilities along the Mid-Atlantic Ridge between 10° and 24° N. Geochemical, Geophysics and Geosystems, 7, Q12010, doi:10.1029/2006GC001317.

Karakaya, N. and Karakaya, M.C. (2001) Hydrothermal alteration of the Saplica volcanic rocks, Sebinkarahisar, Turkey. International Geology Review, 43, 953-962,

Nakamura, D., Kobayashi, T., Shimobayashi, N., Svojtka, M., and Hirajima, T. (2010) Sr-sulphate and associated minerals in kyanite-bearing eclogite in the Moldanubian Zone of the

310 Bohemian Massif, Czech Republic. Journal of Mineralogical and Petrological Sciences, 105,
311 251-261.

312 Nickschick, t., Kämpf, H., and Jahr, T, (2014) The "Triasscholle" near Greiz, Germany—a
313 volcanic origin? Bulletin of Volcanology, 76, 806- , doi:10.1007/s00445-014-0806-x.

314 Rhodes, J.M. and Vollinger, M.J. (2004) Composition of basaltic lavas sampled by phase-2 of
315 the Hawaii Scientific Drilling Project: geochemical stratigraphy and magma types.
316 Geochemistry, Geophysics, Geosystems, 5, doi.org/10.1029/2002GC000434Q03G13.

317 Rukhlov, A.S., Blinova, A.I., and Pawlowicz, J.G. (2013) Geochemistry, mineralogy and
318 petrology of the Eocene potassic magmatism from the Milk River area, southern Alberta, and
319 Sweet Grass Hills, northern Montana. Chemical Geology, 353, 280–302.

320 Singer, D.M., Griffith, E.M., Senko, J.M., Fitzgibbon, K. and Widanagamage, I.H. (2016)
321 Celestine in a sulfidic spring barite deposit — A potential biomarker? Chemical Geology, 442,
322 1–10.

323 U.S. Geological Survey, 2019, Mineral commodity summaries 2019. U.S. Geological Survey,
324 200 p., doi.org/10.3133/70202434.

325 *Xu, C.* Jindrich Kynicky, J., Chakhmouradian, A.R., Qi, L., Song. W. *(2010)* A unique Mo deposit
326 associated with carbonatites in the Qinling orogenic belt, central China. Lithos, 118, 50-60.

327

This is a preprint, the final version is subject to change, of the American Mineralogist (MSA)
Cite as Authors (Year) Title. American Mineralogist, in press.
DOI: https://doi.org/10.2138/am-2020-6995

FIGURE CAPTIONS

1. Map of northern Hawaiian Islands (Kauaʻi, Niʻihau and Kaʻula shown in green). Kaʻula Island is a tuff cone remnant (small green patch on the south side of Kaʻula shield volcano) capping a small, independent Hawaiian shield volcano (Garcia et al., 1986; 2016).

2. Backscattered electron images of celestine (bright areas) in Kaʻula basalt KA-19. (a and b) Vesicles partially to completely filled with celestine (Cs, bright) and the zeolite (zeo) phillipsite. Boxed area in image b was X-ray mapped (Fig. 3). (c) Microporosity surrounding the vesicles also filled with celestine (upper central area in image 2a. (d) Fresh olivine etched by percolating fluids adjacent to celestine-rich area (bright patches). Olivine crystals away from celestine patches are devoid of such wedge-shaped etchings. Cpx; clinopyroxene-rich matrix was apparently unaffected by celestine-bearing solution.

3. Backscattered electron image (BSE) and X-ray maps for Ba and Sr in a celestine aggregate shown in boxed area on Fig. 2c. Ba enrichments (brighter areas) in parallel bands suggest crystallographic control of these areas during celestine growth.

4. Trace element variation diagram for Kaʻula Island accidental basalts. The abundance of the trace elements is normalized to an average, unaltered submarine Kaʻula basalts of similar composition to the island basalt (see Table 2). Elements are plotted in order of decreasing degree of incompatibility in Hawaiian magmas from left to right. Analytical error is smaller than the symbol size. Samples are listed in the legend from least altered at the bottom and in cooler colors (light blue and green) to most altered in warmer colors (yellow-orange-red) based on LOI values (Table 2). The samples with lower and intermediate LOI values (0.2 to 2.1 wt.%) show mild Ba enrichments reflecting presence of Ba-rich zeolites. All of the samples except the least altered one (KA-16) show Rb loss relative to the unaltered submarine sample. The sample with the highest LOI (KA-19 with 4.7 wt.%) has the highest Sr and lowest Ba contents. Paradoxically, this sample also has the lowest Nb and Y contents but nearly the same Ti and Zr contents as the other samples.

This is a preprint, the final version is subject to change, of the American Mineralogist (MSA)
Cite as Authors (Year) Title. American Mineralogist, in press.
DOI: https://doi.org/10.2138/am-2020-6995

Table 1. Representative analyses of celestine in Kaula accidental block KA-19 with cations assuming 4 oxygens

Grain	SiO_2	SrO	BaO	FeO*	CaO	SO_3	Total	Si	Sr	Ba	Fe	Ca	S	Total
1-2	0.01	55.3	0.11	0.39	0.75	42.7	99.2	0.000	0.992	0.001	0.010	0.025	0.990	2.018
2-3	0.03	53.6	0.58	0.27	1.08	44.9	100.5	0.001	0.929	0.007	0.007	0.035	1.007	1.985
2-4	0.29	51.4	1.90	0.51	2.51	42.7	99.3	0.009	0.915	0.023	0.013	0.083	0.983	2.017
2-5	0.52	52.6	1.65	0.57	1.22	42.4	99.0	0.016	0.943	0.020	0.015	0.040	0.983	2.001
3-3	0.10	54.1	0.59	0.20	0.75	44.9	100.6	0.003	0.938	0.007	0.005	0.024	1.007	1.981
3-3	0.15	52.8	0.35	0.30	0.62	44.8	99.0	0.005	0.922	0.004	0.007	0.020	1.012	1.965
5-3	0.37	52.0	2.26	0.06	1.80	43.6	100.1	0.011	0.914	0.027	0.002	0.059	0.992	1.994
11-1	0.23	53.0	1.25	0.47	1.39	43.2	99.6	0.007	0.939	0.015	0.012	0.046	0.992	2.004
13-1	0.05	53.5	2.37	0.46	0.97	43.2	100.5	0.001	0.949	0.028	0.012	0.032	0.992	2.013
13-2	0.00	50.3	4.84	0.34	1.35	43.0	99.9	0.000	0.901	0.059	0.009	0.045	0.995	2.009
13-3	0.06	52.5	1.98	0.34	1.38	42.9	99.2	0.002	0.937	0.024	0.009	0.046	0.993	2.009
13-4	0.02	53.7	0.91	0.44	1.71	43.3	100.1	0.001	0.948	0.011	0.011	0.056	0.991	2.017
13 dark	0.11	51.0	2.43	0.37	1.98	42.9	98.8	0.004	0.911	0.029	0.010	0.066	0.992	2.008
13 bright	0.94	47.0	7.50	0.36	1.35	42.9	100.1	0.029	0.837	0.090	0.009	0.044	0.987	1.967
14-1	0.07	50.7	4.08	0.43	1.16	43.1	99.6	0.002	0.906	0.049	0.011	0.038	0.997	2.001
celestine std. ave.	0.04	56.4	0.08	0.00	0.00	43.7	100.1	0.001	0.997	0.001	0.000	0.000	1.000	1.998
celestine std. given	0.00	56.4	0.10	0.00	0.00	43.6	100.1	0.001	1.000	0.001	0.000	0.000	1.000	2.001

*FeO as total iron

This is a preprint, the final version is subject to change, of the American Mineralogist (MSA)
Cite as Authors (Year) Title. American Mineralogist, in press.
DOI: https://doi.org/10.2138/am-2020-6995

Table 2. New XRF analyses of Kaula lithic basaltic blocks with comparison to basanitic Kaula submari

Sample	SiO_2	TiO_2	Al_2O_3	Fe_2O_3*	MnO	MgO	CaO	Na_2O	K_2O	P_2O_5	Total	LOI	Nb	Ba	Rb
Accidental island blocks															
KA-15	42.18	2.73	11.53	14.32	0.22	13.38	10.44	3.31	1.16	0.70	99.95	0.42	52.8	663	28.1
KA-31	40.97	2.83	12.03	14.20	0.23	12.83	10.85	3.74	1.23	0.86	99.77	0.53	48.9	757	29.9
KA-28	42.42	2.83	12.55	14.60	0.22	10.44	10.67	3.75	1.49	0.74	99.72	0.65	55.7	825	33.0
KA-34	40.89	2.83	11.91	14.74	0.33	11.87	12.62	2.52	1.35	0.87	99.92	2.13	51.4	860	24.9
KA-17	41.49	2.62	11.94	14.23	0.25	12.41	11.41	3.35	1.22	1.13	100.04	1.78	55.2	947	19.6
KA-19	42.79	2.73	12.12	13.97	0.20	12.71	11.53	1.75	1.27	0.69	99.76	2.82	40.2	494	20.7
Submarine pillow basalts^															
J2-304-21	41.63	2.59	12.69	13.82	0.22	11.56	11.29	3.89	1.46	0.77	99.92	0.27	50.4	705	32.5
J2-304-22	41.77	2.55	12.30	13.94	0.25	12.14	11.18	3.72	1.41	0.74	100.00	0.32	48.5	646	31.5
J2-304-23	41.76	2.59	12.67	13.65	0.22	11.63	11.41	3.86	1.43	0.77	99.99	0.45	50.0	688	31.0
average	41.72	2.58	12.55	13.80	0.23	11.78	11.29	3.82	1.43	0.76	99.97	0.35	49.6	680	31.7

*Total iron; ^data from Garcia et al. (2016)

This is a preprint, the final version is subject to change, of the American Mineralogist (MSA)
Cite as Authors (Year) Title. American Mineralogist, in press.
DOI: https://doi.org/10.2138/am-2020-6995

ne basalts

Sr	Y	Zr	Zn	Ni	Cr	V
1247	20.0	143	108	429	457	290
1376	22.0	161	118	360	477	293
1969	21.0	215	126	228	277	270
2274	21.0	151	114	294	366	281
2380	24.0	180	115	295	412	279
6404	18.0	106	106	311	428	286
1210	21.7	169	116	264	345	259
1154	21.9	169	116	261	352	262
1204	22.0	167	113	267	369	256
1189	21.9	168	115	264	355	259

This is a preprint, the final version is subject to change, of the American Mineralogist (MSA)
Cite as Authors (Year) Title. American Mineralogist, in press.
DOI: https://doi.org/10.2138/am-2020-6995

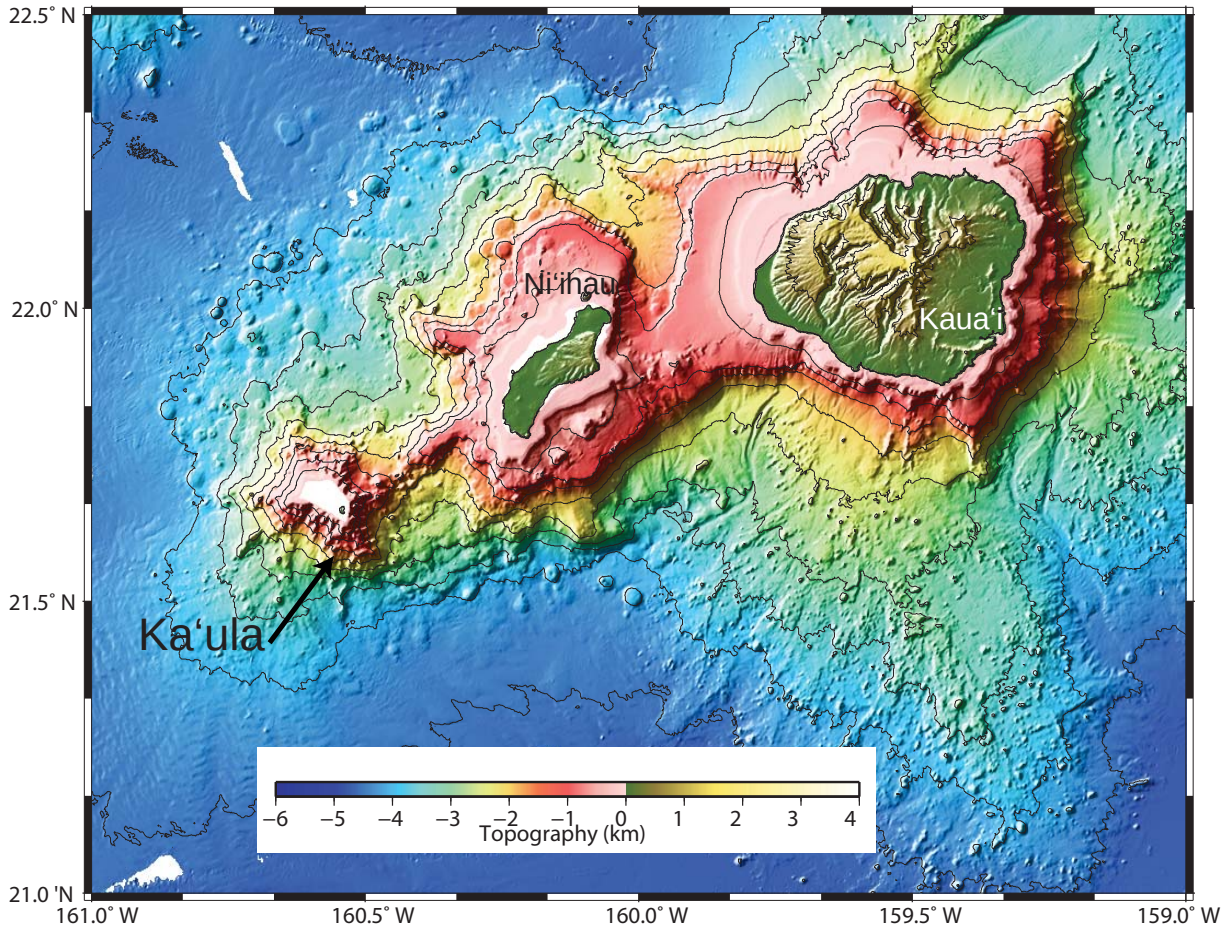

This is a preprint, the final version is subject to change, of the American Mineralogist (MSA)
Cite as Authors (Year) Title. American Mineralogist, in press.
DOI: https://doi.org/10.2138/am-2020-6995

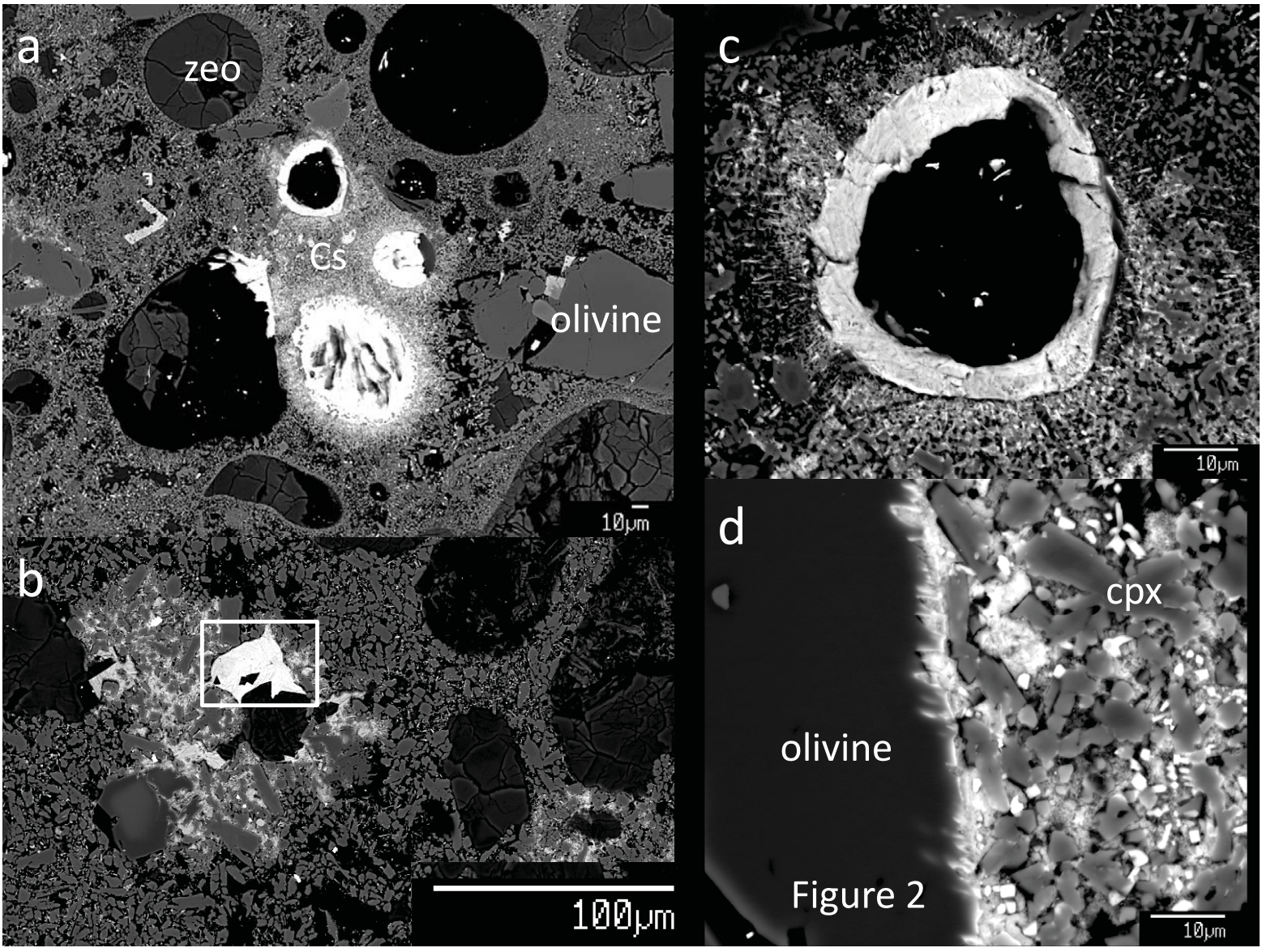

Figure 2

This is a preprint, the final version is subject to change, of the American Mineralogist (MSA)
Cite as Authors (Year) Title. American Mineralogist, in press.
DOI: https://doi.org/10.2138/am-2020-6995

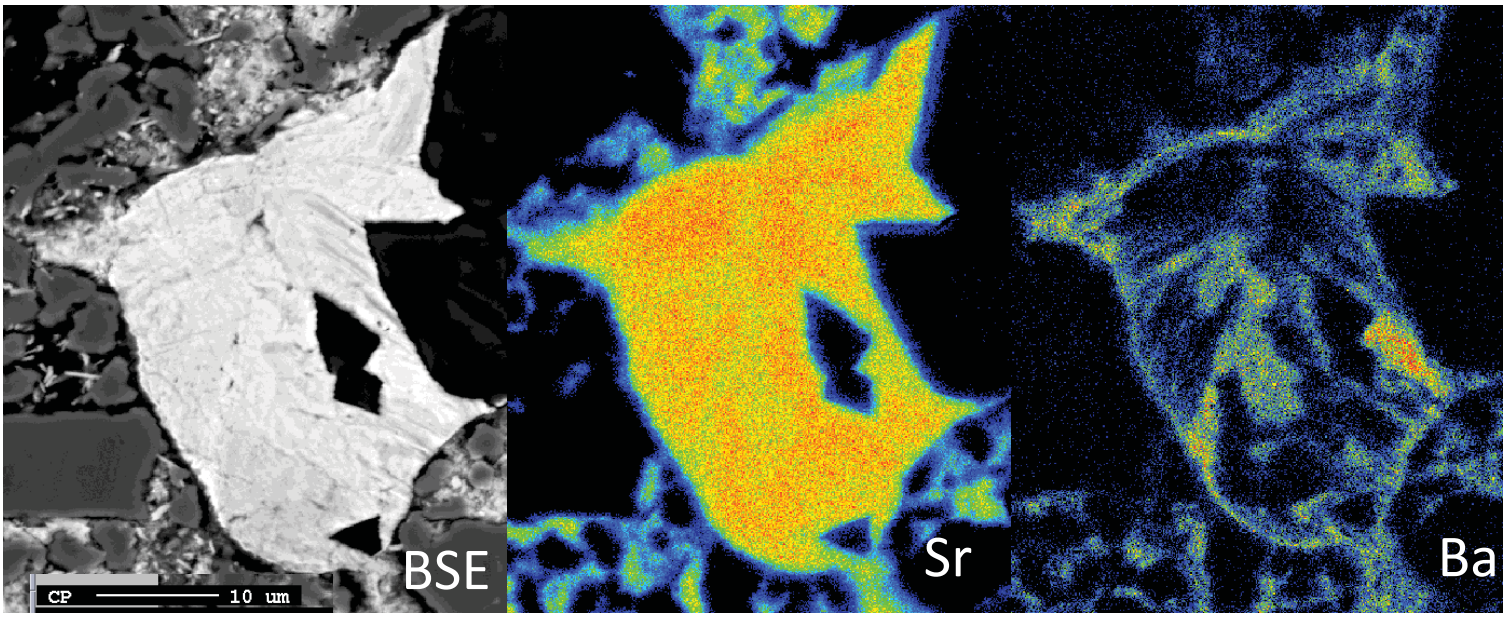

Figure 3 Garcia and Hellebrand

This is a preprint, the final version is subject to change, of the American Mineralogist (MSA)
Cite as Authors (Year) Title. American Mineralogist, in press.
DOI: https://doi.org/10.2138/am-2020-6995

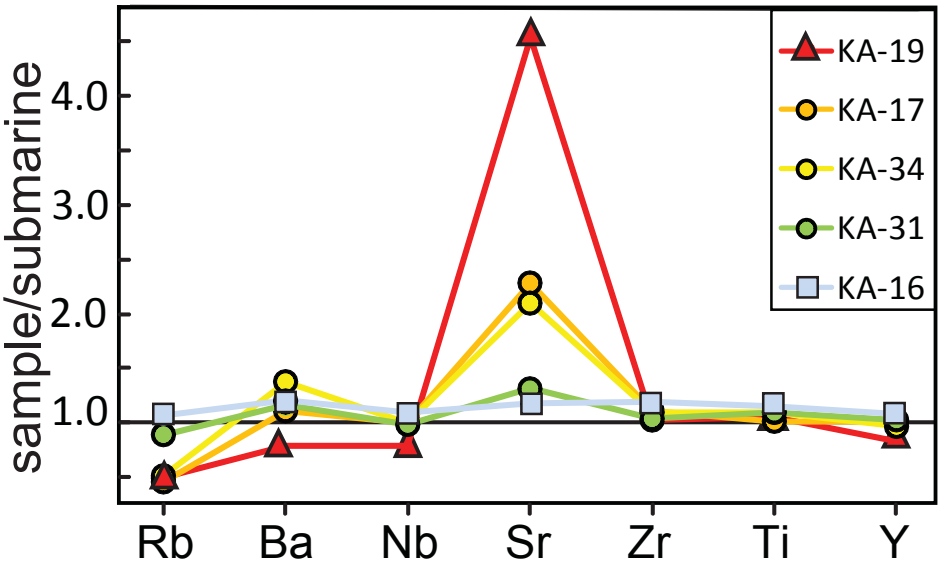

Fig. 4 Garcia and Hellebrand